

# Controlling fusion at astrophysical energies through the electrons chaotic motion

Sachie Kimura<sup>a</sup> and Aldo Bonasera<sup>a</sup>

<sup>a</sup>*Laboratorio Nazionale del Sud, INFN, via Santa Sofia, 62, 95123 Catania, Italy*

---

## Abstract

We perform semi-classical molecular dynamics simulations of screening by bound electrons in low energy nuclear reactions. In our simulations quantum effects corresponding to the Pauli and Heisenberg principle are enforced by constraints. In addition to the well known adiabatic and sudden limits, we propose a new "dissipative limit" which is expected to be important not only at high energies but in the extremely low energy region. The dissipative limit is associated with the chaotic behavior of the electronic motion. It affects also the magnitude of the enhancement factor. We discuss also numerical experiments using polarized targets. The derived enhancement factors in our simulation are in agreement with those extracted within the  $R$ -matrix approach.

*Key words:*

---

## 1 Introduction

The relation between the tunneling process and dynamical chaos has been discussed with great interests in the field of nonlinear science (1; 2). Though tunneling is a completely quantum mechanical phenomenon, it might be influenced by classical chaos. In the sense that chaos induces fluctuations on the classical action which essentially determines the tunneling probability. We study the phenomenon by examining the screening effects by bound electrons in low energy fusion reactions, where the experimental cross sections with gas targets show an increasing enhancement with decreasing bombarding energy with respect to the values obtained by extrapolating from the data at high energies (3; 4). Many studies attempted to attribute the enhancement of the reaction rate to the screening effects by bound target electrons (5). In this context one often estimates the screening potential( $U_e$ ) as a constant decrease of the barrier height in the tunneling region through a fit to the data. A puzzle has been that the screening potential obtained by this procedure exceeds the

value of the adiabatic limit, which is given by the difference of the binding energies of the united atoms and of the target atom and it is theoretically thought to provide the maximum screening potential (6). The experiments have been performed using deuterated metallic targets, as well, and it is reported that one observes systematically large screening potentials for various kinds of metals (7).

The difficulty lies in the determination of the absolute value of the bare cross section. The extrapolated bare cross section, i.e., the astrophysical S-factor, might be affected by the choice of the high energy region where one assumes the screening potential can be neglected (8). Over these years, several ways to determine the bare cross sections have been proposed. There are theoretical attempts, using  $R$ -matrix theory (9), and experimental, using the Trojan Horse Method (THM) (10; 11). However, the THM gives only relative values of the S-factors and one needs to normalize to direct methods data obtained at high incident energies. Thus the comparison between newly obtained bare cross sections and the cross sections by the direct measurements gives a variety of values for the screening potential. These values are often smaller than the sudden limit or larger than the adiabatic limit. Theoretical studies performed using the time-dependent Hartree-Fock (TDHF) scheme (12; 13) suggest that the screening potential is between the sudden and the adiabatic limits.

One of the aims of this paper is to try to assess the effect of the screening quantitatively. Up to now, the dynamical effects of bound electrons have been studied only in some limited cases with a few bound electrons ( $D+d$  with atomic target (12; 13) and molecular target (14),  ${}^3\text{He}+d$  (12)) with the TDHF method. We investigate here the dynamical effects, including the tunneling region, for other systems with many bound electrons;  $D+D$ ,  ${}^3\text{He}+D$ , looking the effect of the electron capture of projectile,  ${}^6\text{Li}+d$ ,  ${}^6\text{Li}+D$ .

To simulate the effects of many electrons, we use the constrained molecular dynamics (CoMD) model (2; 15; 16). At very low energies fluctuations are anticipated to play a substantial role. Molecular dynamics contains all possible correlations and fluctuations due to the initial conditions (events). The prescription using constraints for the Heisenberg uncertainty principle and the Pauli exclusion principle is based on the Lagrange multiplier method (16). In extending the study to lower incident energies, we would like to stress the connection between the motion of bound electrons and chaos. In fact, depending on the dynamics, the behavior of the electron(s) is unstable and influences the relative motion of the projectile and the target. This feature is caused by the nonintegrability of the 3-body system and it is well known that the tunneling probability can be modified by the existence of a chaotic environment. In this connection we propose a new “dissipative limit” which is driven by electron ejection. We examine also numerical experiments using polarized targets.

The paper is organized as follows. In sect. 2 we introduce the enhancement factor  $f_e$  and describe the essence of the constrained molecular dynamics approach briefly. In sect. 3 we mention limiting cases where one can easily estimate the screening energy. We discuss particular reactions, the effect of the electron capture by projectile and the numerical experiments using polarized targets. We summarize the paper in sect. 4.

## 2 Formalism

We denote the reaction cross section at incident energy in the center of mass  $E$  by  $\sigma(E)$  and the cross section obtained in absence of electrons by  $\sigma_0(E)$ . The enhancement factor  $f_e$  is defined as

$$f_e \equiv \frac{\sigma(E)}{\sigma_0(E)}. \quad (1)$$

If the effect of the electrons is well represented by the constant shift  $U_e$  of the potential barrier,  $\sigma(E)$  is replaced by  $\sigma_0(E + U_e)$  following (12; 17),

$$f_e \sim \exp \left[ \pi \eta(E) \frac{U_e}{E} \right], \quad (2)$$

where  $\eta(E)$  is the Sommerfeld parameter (18). We calculate the enhancement factor through the CoMD simulation.

### 2.1 Constrained Molecular Dynamics

We describe the essence of CoMD briefly. The total Hamiltonian is written down as

$$H(\mathbf{r}; \mathbf{p}) = \sum_i^N (\mathcal{E}_i + U(\mathbf{r}_i) - m_i c^2), \quad (3)$$

where we use relativistic kinematics:  $\mathcal{E}_i = \sqrt{\mathbf{p}_i^2 c^2 + m_i^2 c^4}$ ,  $m_i$  and

$$U(\mathbf{r}_i) = \sum_{j(\neq i)=0}^N \frac{q_j q_i}{|\mathbf{r}_i - \mathbf{r}_j|} \quad (4)$$

are the energy, the mass and the potential of the  $i$ -th particle, i.e., an electron or a nucleus, respectively. Here,  $q_i$  is the charge of the particle  $i$ . In classical molecular dynamics(CMD) one solves the Hamilton equations, i.e.,:

$$\frac{d\mathbf{r}_i}{dt} = \frac{\mathbf{p}_i c^2}{\mathcal{E}_i}; \quad \frac{d\mathbf{p}_i}{dt} = -\nabla_{\mathbf{r}} U(\mathbf{r}_i), \quad (5)$$

The initial configurations of the bound electrons are prepared using CoMD, as well (16). To take the feature of the Pauli blocking into account, we use the Lagrange multiplier method for constraints. Our constraints which correspond to the Pauli blocking is  $\bar{f}_i \leq 1$  in terms of the occupation probability and can be directly related to the distance of two particles, i.e.,  $r_{ij} p_{ij}$ , in the phase space. Here  $r_{ij} = |\mathbf{r}_i - \mathbf{r}_j|$  and  $p_{ij} = |\mathbf{p}_i - \mathbf{p}_j|$ . The relation  $\bar{f}_i \leq 1$  is fulfilled, if  $r_{ij} p_{ij} \geq \xi_P \hbar \delta_{s_i, s_j}$ , where  $\xi_P = 2\pi(3/4\pi)^{2/3} 2^{1/3}$ ,  $i, j$  refer only to electrons and  $s_i, s_j (= \pm 1/2)$  are their spin projection. We can easily extend the approach to the Heisenberg principle where the constraint is expressed as  $r_{ij} p_{ij} \geq \xi_H \hbar$ , and  $\xi_H = 1$ ,  $i$  and  $j$  refer to the electrons and to the nuclei. Using these constraints, the Lagrangian of the system can be written as

$$\mathcal{L} = \sum_i^N \mathbf{p}_i \cdot \dot{\mathbf{r}}_i - H(\mathbf{r}; \mathbf{p}) + \sum_{i,j(i)} \lambda_i^H \left( \frac{r_{ij} p_{ij}}{\xi_H \hbar} - 1 \right) + \sum_{i,j(i)} \lambda_i^P \left( \frac{r_{ij} p_{ij} \delta_{s_i, s_j}}{\xi_P \hbar} - 1 \right), \quad (6)$$

where  $\lambda_i^P$  and  $\lambda_i^H$  are Lagrange multipliers for Pauli and Heisenberg principle respectively. The variational calculus leads to:

$$\frac{d\mathbf{r}_i}{dt} = \frac{\mathbf{p}_i c^2}{\mathcal{E}_i} + \frac{1}{\hbar} \sum_{j(i)} \left( \frac{\lambda_i^H}{\xi_H} + \frac{\lambda_i^P}{\xi_P} \delta_{s_i, s_j} \right) r_{ij} \frac{\partial p_{ij}}{\partial \mathbf{p}_i}, \quad (7)$$

$$\frac{d\mathbf{p}_i}{dt} = -\nabla_{\mathbf{r}} U(\mathbf{r}_i) - \frac{1}{\hbar} \sum_{j(i)} \left( \frac{\lambda_i^H}{\xi_H} + \frac{\lambda_i^P}{\xi_P} \delta_{s_i, s_j} \right) p_{ij} \frac{\partial r_{ij}}{\partial \mathbf{r}_i}. \quad (8)$$

where  $\lambda_i^P$  and  $\lambda_i^H$  are zero, if the two particles  $i$  and  $j$  are far separated;  $r_{ij} p_{ij} \geq \xi \hbar$  ( $\xi = \xi_P$  for electrons  $i$  and  $j$ , which have identical spin projections and  $\xi = \xi_H$  for the other pairs of particles). In this case the eqs. (7) and (8) redeem the eqs. (5). The integration of the eqs. (7) and (8) is performed using Hermite integration scheme which is efficient and capable of high precision. The scheme adopts variable and individual time-steps for each electron and nucleus (19). The Lagrange multipliers are used to obtain the ground states of atomic nuclei. During the collision we set the  $\lambda_i \equiv 0$  to conserve energy. If needed, a collision term among electrons is introduced to avoid the over occupancy of the phase space (15). For the collisions reported here we found the violation of the Heisenberg and Pauli principles negligible during the collision dynamics.

The importance of the influence of the tunneling region to the electron screening has been discussed in (13). In order to treat the tunneling process in the CoMD framework, we define the collective coordinates  $\mathbf{R}^{coll}$  and the collective momentum  $\mathbf{P}^{coll}$  as

$$\mathbf{R}^{coll} \equiv \mathbf{r}_P - \mathbf{r}_T; \quad \mathbf{P}^{coll} \equiv \mathbf{p}_P - \mathbf{p}_T, \quad (9)$$

where  $\mathbf{r}_T, \mathbf{r}_P$  ( $\mathbf{p}_T, \mathbf{p}_P$ ) are the coordinates(momenta) of the target and the projectile nuclei, respectively. When the collective momentum becomes zero, we switch on the collective force, which is determined by  $\mathbf{F}_P^{coll} \equiv \dot{\mathbf{P}}^{coll}$  and  $\mathbf{F}_T^{coll} \equiv -\dot{\mathbf{P}}^{coll}$ , to enter into imaginary time (20). We follow the time evolution in the tunneling region using the equations,

$$\frac{d\mathbf{r}_{T(P)}^{\Im}}{d\tau} = \frac{\mathbf{p}_{T(P)}^{\Im}}{\mathcal{E}_{T(P)}}; \quad \frac{d\mathbf{p}_{T(P)}^{\Im}}{d\tau} = -\nabla_{\mathbf{r}}U(\mathbf{r}_{T(P)}^{\Im}) - 2\mathbf{F}_{T(P)}^{coll}, \quad (10)$$

where  $\tau$  is used for imaginary time to be distinguished from real time  $t$ .  $\mathbf{r}_{T(P)}^{\Im}$  and  $\mathbf{p}_{T(P)}^{\Im}$  are position and momentum of the target (the projectile) during the tunneling process respectively. In fact in the tunneling region the path which gives an important contribution to the action of Feynman path integral lies in the imaginary time region. The path coincides with the classical path in the potential valley which is given by turning the barrier upside down (21).

The penetrability of the barrier is given by (20)

$$\Pi(E) = (1 + \exp(2\mathcal{A}(E)/\hbar))^{-1}, \quad (11)$$

where the action integral  $\mathcal{A}(E)$  is

$$\mathcal{A}(E) = \int_{r_b}^{r_a} \mathbf{P}^{coll} d\mathbf{R}^{coll}, \quad (12)$$

$r_a$  and  $r_b$  are the classical turning points. The internal classical turning point  $r_b$  is determined using the sum of the radii of the target and projectile nuclei. Similarly from the simulation without electron, we obtain the penetrability of the bare Coulomb barrier  $\Pi_0(E)$ . Since nuclear reaction occurs with small impact parameters on the atomic scale, we consider only head on collisions. The enhancement factor is thus given by eq. (1),

$$f_e = \Pi(E)/\Pi_0(E) \quad (13)$$

for each event in our simulation. Thus we have an ensemble of  $f_e$  values at each incident energy.

### 3 Applications to Electron Screening Problem

We investigate the enhancement factor for  $D+d$ ,  $D+D$ ,  ${}^3\text{He}+d$ ,  ${}^3\text{He}+D$ ,  ${}^6\text{Li}+d$ ,  ${}^6\text{Li}+D$  reactions. It is well known that in the low incident energy region the projectile often captures electrons before it collides with the target nucleus. The atomic projectile cases ( $D+D$ ,  ${}^3\text{He}+D$ ,  ${}^6\text{Li}+D$ ) in contrast with the bare ionic beam projectile cases ( $D+d$ ,  ${}^3\text{He}+d$ ,  ${}^6\text{Li}+d$ ) reveal the effect of the extra electrons.

#### 3.1 Two well known limits and the Dissipative limit

As it is often discussed in the literature, there are two limiting cases where one can easily estimate the screening potential  $U_e$ . One is the adiabatic and the other is the sudden limit (5). In the sudden limit one assumes that the relative velocity of the two ions is relatively faster than that of the electrons, so that the bound electrons remain frozen during the reaction. Instead in the adiabatic limit which is associated with the slow relative velocity limit, the electrons change their configurations following the relative motion of ions. Especially in the case where the electrons occupy the ground state of the system at the beginning of the reaction, the electrons tend to continue occupying the ground state throughout the reaction process. Effectively the electrons move close to the target nucleus during the collision. In such a way the electrons continue to shield the coulomb repulsive field between the target and the projectile. In this limit the screening potential is given by the difference between the binding energies of the target ( $B.E.^{(T)}$ ) and the united atom ( $B.E.^{(UA)}$ ) which is formed in the last stage of the reaction,

$$U_e^{(AD)} = B.E.^{(T)} - B.E.^{(UA)}. \quad (14)$$

We propose another case which is obtained as a result of the bound electron emission. It gives usually a negative effect to the fusion enhancement, because the electrons take the kinetic energy away from the ions relative motion. We name the new limit as "dissipative limit" (DL). The screening potential in the dissipative limit is given by

$$U_e^{(DL)} = B.E.^{(T)}, \quad (15)$$

where we assume that the ejected electron has zero kinetic energy. If the electron takes finite kinetic energy away, the screening potential can be smaller than the dissipative limit. Note that  $U_e^{(DL)}$  has a negative value. Such a phenomenon seldom occur in the framework of the mean field approach such as

TDHF because of the usually assumed spherical symmetry of the system. We would like to stress here that the DL could be used to perform low energy collisions using relatively higher energy beams, similar in some sense to the THM. In fact we propose to perform experiments where the fusion residues are detected in coincidence with energetic electrons. Thus increasing the value of the ejected kinetic energy of the electrons is as if decreasing the beam energy.

### 3.2 Reactions

#### 3.2.1 $D+d$ and $D+D$ reactions

Fig. 1 shows the incident energy dependence of the enhancement factor for the  $D+d$  and  $D+D$  reactions, where the systems involve 1 and 2 electrons respectively. The open and closed squares show the average enhancement factors

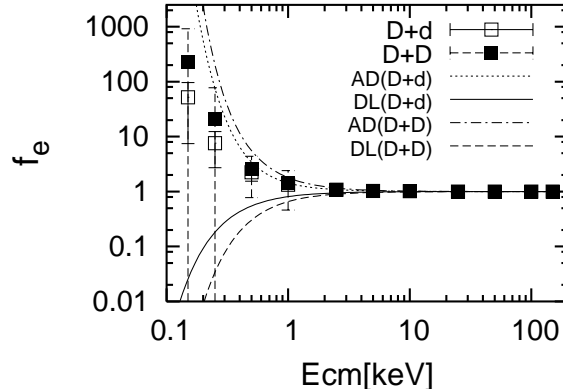


Fig. 1. Enhancement factor as a function of incident center-of-mass energy for the  $D+d$  and  $D+D$  reactions.

$\bar{f}_e$  over events for the  $D+d$  and  $D+D$  reactions, respectively. The variances  $\Sigma = (\bar{f}_e^2 - (\bar{f}_e)^2)^{1/2}$  are shown with error bars. The dotted and dash-dotted curves show the enhancement factors in the adiabatic limit  $f_e^{(AD)}$  for an atomic deuterium target and it is obtained by assuming equally weighted linear combination of the lowest-energy gerade and ungerade wave function for the electron, reflecting the symmetry in the  $D+d$ , i.e.,

$$f_e^{(AD)} = \frac{1}{2} \left( e^{\pi\eta(E)\frac{U_e^{(g)}}{E}} + e^{\pi\eta(E)\frac{U_e^{(u)}}{E}} \right), \quad (16)$$

where  $U_e^{(g)} = 40.7$  eV and  $U_e^{(u)} = 0.0$  eV (13; 12) for  $D+d$  case. If we take into account the electron capture of the projectile, i.e., in the case of  $D+D$ ,

the enhancement factor in the adiabatic limit is

$$f_e^{(AD)} = \frac{1}{4}e^{\pi\eta(E)\frac{U_e^{(g.s.)}}{E}} + \frac{3}{4}e^{\pi\eta(E)\frac{U_e^{(1es)}}{E}}, \quad (17)$$

where  $U_e^{(g.s.)} = 51.7$  eV and  $U_e^{(1es)} = 31.9$  eV (22). The solid curve and dashed curve show the enhancement factors in the dissipative limit  $f_e^{(DL)}$  for D+d and D+D reactions respectively. Notice how the calculated enhancement factor with their variances nicely ends up between the adiabatic and the dissipative limits. We performed also a fit of our data using eq. (2) including the very low energy region and obtained  $U_e = 15.9 \pm 2.0$  eV for D+d case and  $U_e = 21.6 \pm 0.3$  eV for D+D reaction.

In Fig.1 we saw the rough property of the enhancement factors as average values and their variances. Now we discuss their distributions for the D+d reaction. Fig. 2 shows the histograms of the normalized enhancement factors ( $f_e/\bar{f}_e$ ) at the incident energies  $E_{cm} = 0.25$ keV (top panel), 2.5keV (middle panel) and 100keV (bottom panel). The stars, open squares and crosses specify the adiabatic, sudden and dissipative limits at each incident energy, respectively. A remarkable feature in those figures is that at the highest incident energy, the enhancement factor for each event in an ensemble distribute almost as a  $\delta$ -function around the average enhancement factor. As the incident energy goes down, it spreads around the average and the adiabatic limit at  $E_{cm} = 2.5$ keV. However, at the lowest incident energy  $E_{cm} = 0.25$ keV, where any experiment has not reached yet, instead one can see clearly that the distribution of the enhancement factor changes and the peak of the distribution approaches the dissipative limit. At a glance it appears strange that the enhancement factor goes to the dissipative limit (which we expected to be important in the high incident energy region) and plays a key role at such a low energy. The phenomenon can be interpreted due to the chaotic behavior of the bound electrons in the many-body systems(2; 23), which becomes important especially in the extremely low energy reactions, where the interaction time is relatively long and the electrons have enough time to interact with the projectile ions.

To strengthen the finding of the electrons influence on the enhancement factor, in Fig. 3 we show the enhancement factors for many events as a function of the electrons binding energy at the external classical turning point. As one can see, there is a clear correlation. In fact the larger the electrons binding energy, the higher the enhancement factor is. Thus in order to control the fusion probability we need to have some control on the electronic motion especially at low energies as we describe next.

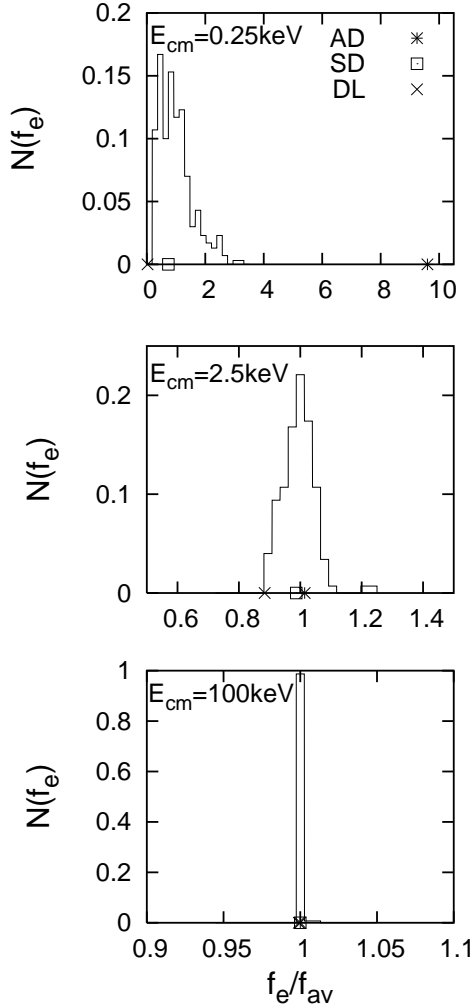


Fig. 2. Histograms of the normalized enhancement factor for the D+d reaction at various incident energies. In the figure stars, open squares and crosses shows the adiabatic, sudden and dissipative limits, respectively.

### 3.2.2 Polarized targets

We prepared numerically ensembles of target atoms where the electrons motion is polarized perpendicular  $P_{\perp}$  or parallel  $P_{\parallel}$  to the beam axis. Fig. 4 shows the initial configuration dependence of the enhancement factor at the incident energy  $E_{cm} = 1.25\text{keV}$ . The open circles are the enhancement factors for  $P_{\perp}$  targets and the closed squares are the ones for  $P_{\parallel}$  targets. It is clear that the  $P_{\perp}$  targets give always large enhancement factors and a small variance, as it is shown with the error bars in the figure. Instead the  $P_{\parallel}$  targets give relatively small enhancement factors and large variances. As we mentioned in the reference (2) or it is discussed in the reference (23) as an example of the coplanar collisions, this is the case where the oscillational force mostly affects the relative motion between the two nuclei. Because of the non-integrability

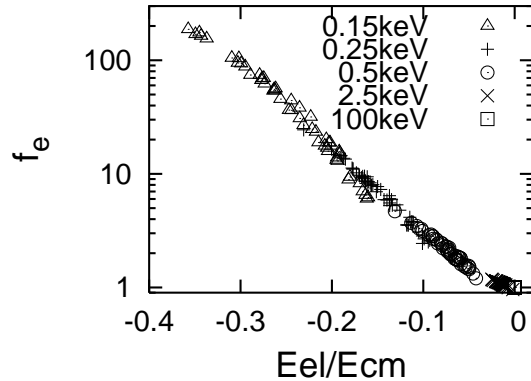


Fig. 3. The enhancement factor as a function of the binding energies of the electron at the external classical turning point divided by the incident energies for the D+d reaction.

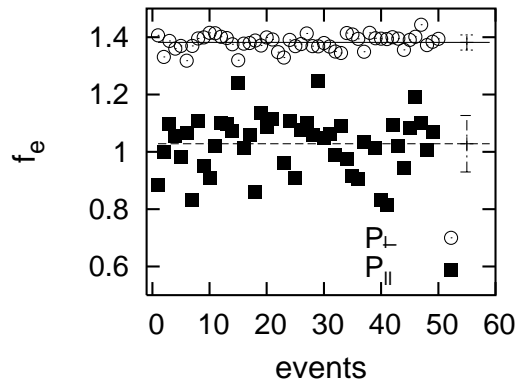


Fig. 4. The initial configuration dependence of the enhancement factor at the incident energy  $E_{cm} = 1.25\text{keV}$ . The enhancement factors for  $P_{\perp}$  targets (open circles) and for  $P_{\parallel}$  targets (closed squares) are shown.

of the system under such a force, the motion of the electron becomes unstable and it is often ejected to the continuum state. Notice that it corresponds to the dissipative limit which we defined in this paper. The large variance of the  $P_{\parallel}$  targets originates from the fact that the chaotic behavior of the system affects the determination of the enhancement factor. A remarkable feature is that with the  $P_{\parallel}$  targets the enhancement factor often becomes less than 1. It means that in this case the bound electron gives an hindrance to the tunneling probability.

In Fig. 5 we show the incident energy dependence of the average enhancement factor for the  $P_{\perp}$  and  $P_{\parallel}$  targets with pluses and crosses, particularly in the low energy region. The enhancement factors from the  $P_{\perp}$  targets are always larger than that from the  $P_{\parallel}$  targets. In contrast to the average enhancement

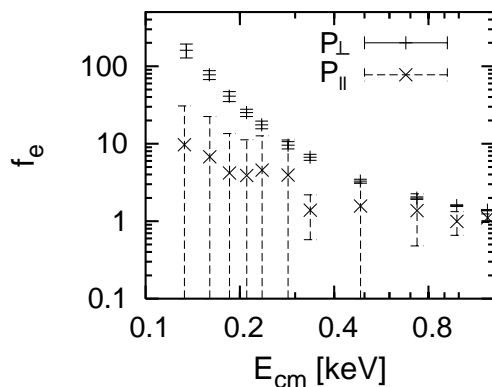


Fig. 5. same as Fig. 1 but for  $P_{\perp}$  and  $P_{\parallel}$  targets.

from the  $P_{\perp}$  targets, which increases monotonically as the incident energy becomes smaller, the average enhancement from the  $P_{\parallel}$  targets fluctuates. It has also large variances at low energies.

In figures 6 and 7 we show the histograms of the enhancement factor for  $P_{\parallel}$  (top panel),  $P_{\perp}$  (bottom panel) at two relatively low incident energies ( $E_{cm} = 1\text{keV}$  and  $0.25\text{keV}$ ). In the abscissa the enhancement factor is normalized with its average value over the ensemble of unpolarized targets.

One notices that at the incident energy  $E_{cm} = 1\text{keV}$  (Fig. 6) the enhancement factor for each events distributes around and close to its average value, which is slightly less than the adiabatic limit, as a comprehensive feature. By looking each panels carefully one sees that the  $P_{\parallel}$  target tends to give smaller enhancement factors than the  $P_{\perp}$  target gives, as it is shown in Fig. 4. There is also some hindrance in the parallel target case.

The change from Fig. 6 to Fig. 7 is drastic. First, all the events are smaller than the adiabatic limit, as we already saw in Fig. 2 for the case of the unpolarized targets. Also using  $P_{\perp}$  targets we obtain enhancement factors always larger than the average value.

### 3.2.3 ${}^3\text{He}+d$ and ${}^3\text{He}+D$ reactions

An excess of the screening potential was reported for the  ${}^3\text{He}+d$  with atomic gas  ${}^3\text{He}$  target, and  $\text{D}_2 + {}^3\text{He}$  reaction with deuterium molecular gas target, for the first time (3). Since then various experiments have been performed for these reactions. The incident energy covers from 5 keV to 50 keV for  ${}^3\text{He}+d$ . Though once the problem of the discrepancy between experimental data and theoretical prediction seemed to be solved by considering the correct energy loss data (24), recent measurements using measured energy loss data (25)

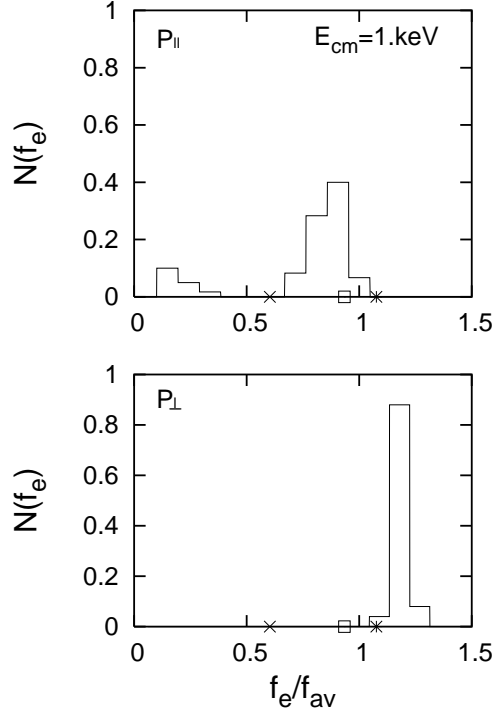


Fig. 6. Histograms of the normalized enhancement factors for the D+d reaction. Incident energy  $E_{cm} = 1. \text{keV}$ , polarized parallel target to the beam axis (top panel) and polarized perpendicular target (bottom panel). Again stars, open squares and crosses indicate the adiabatic, sudden and dissipative limits, respectively.

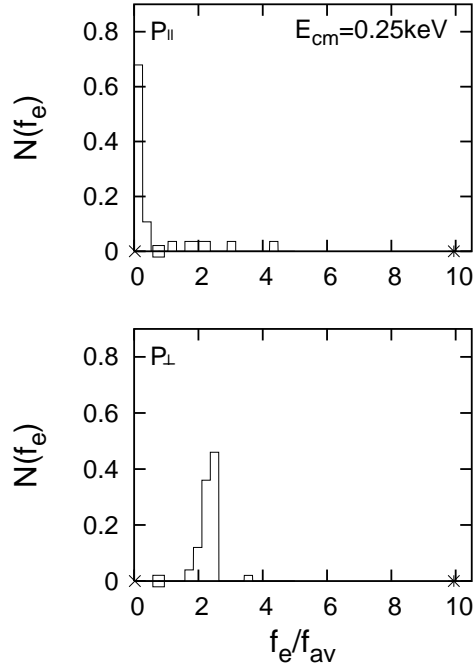


Fig. 7. same with Fig. 6 but at the incident energy  $E_{cm} = 0.25 \text{keV}$ .

report larger screening potentials than in the adiabatic limit for both reactions.

The electron capture by the projectile plays a minor role in the case of  ${}^3\text{He}+d$ , since electrons are more bound in helium targets. However in the recent measurement Aliotta et al. used molecular  $\text{D}_2^+$  and  $\text{D}_3^+$  targets (25). Thus we assess the contribution from  ${}^3\text{He}+D$  reaction, as well.

The enhancement factor in the adiabatic limit for the  ${}^3\text{He}+d$  and  ${}^3\text{He}+D$  reactions give  $U_e=119$  eV for  ${}^3\text{He}+d$  and  $U_e=110$  eV for  ${}^3\text{He}+D$ , respectively. These are shown in the figure 8 with the solid curve for  ${}^3\text{He}+d$  and with the dashed curve for  ${}^3\text{He}+D$ . The comparison of these two adiabatic limits implies that the electron capture of projectile would give a hindrance compared with the bare deuteron projectile. Meanwhile the latest analysis of the experimental data using  $R$ -matrix two level fit (9) suggests the screening potential  $U_e = 60$  eV (corresponding enhancement factor is shown with dotted curve). The comparison between direct measurement and an indirect method, the Trojan Horse method, suggests the screening potential  $U_e = 180\pm 40$  eV (corresponding enhancement factor is shown with dot-dashed curve) (26). The average enhancement factors  $\bar{f}_e$  over events in our simulations using CoMD are shown with the open and closed squares for the  ${}^3\text{He}+d$  and  ${}^3\text{He}+D$  reactions, respectively.

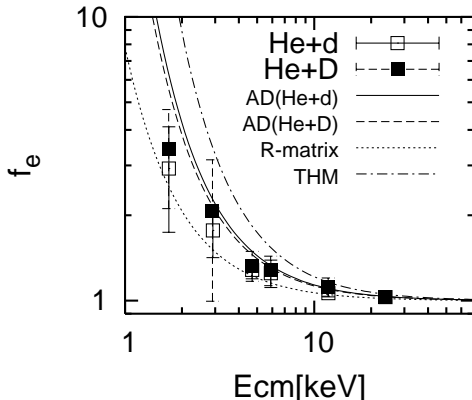


Fig. 8. Enhancement factor as a function of incident center-of-mass energy for the  ${}^3\text{He}+d$  and  ${}^3\text{He}+D$  reactions.

Notice that our calculated enhancement factors for the two systems display an opposite trend as compared to the adiabatic limits. The average enhancement factor of the  ${}^3\text{He}+D$  reaction agrees with the estimation of the adiabatic limit and the  ${}^3\text{He}+d$  reaction is below the corresponding adiabatic limit. The paradoxical feature comes from the fact that an electron between the two ions is often kicked out during the reaction process, i.e., the electron configuration seldom settles down the  ${}^5\text{Li}^+$  ground state. It is known as autoionization in the context of the Classical Trajectory Monte Carlo method (27). Instead in the case of the  ${}^3\text{He}+D$  deuterium projectile bring its bound electron in a tight bound state around the unified nuclei of  ${}^3\text{He}$  and  $d$ , practically it ends up with

ground state configuration of the  ${}^5\text{Li}$  atom. The fit of the obtained enhancement factors suggests the screening potentials  $U_e = 83.2 \pm 1.2$  eV for  ${}^3\text{He}+d$  and  $U_e = 87.4 \pm 5.3$  eV for  ${}^3\text{He}+D$ .

### 3.2.4 ${}^6\text{Li}+d$ reaction

The S-factors for the  ${}^6\text{Li}+d$ ,  ${}^6\text{Li}+p$  and  ${}^7\text{Li}+p$  reactions were measured over the energy range  $10 \text{ keV} < E_{cm} < 500 \text{ keV}$  by Engstler, *et al.* (4). They used LiF solid targets and deuteron projectiles as well as deuterium molecular gas targets and Li projectiles.

In the case of LiF target which is a large band gap insulator, one often approximates the electronic structure of the target  ${}^6\text{Li}({}^7\text{Li})$  state by the  ${}^6\text{Li}^+({}^7\text{Li}^+)$  with only two innermost electrons. Thus for all three reactions one expects the screening potential in the adiabatic limit  $U_e^{(AD)} = 371.8 - 198.2 \sim 174$  eV. Instead if one uses the ground state  ${}^6\text{Li}({}^7\text{Li})$  atom and the bare deuteron target as the initial state,  $U_e^{(AD)} = 186$  eV (5). In Fig. 9 we show the enhancement factor for  $U_e^{(AD)} = 186$  eV with solid curve.

However one should be aware that the deuteron or hydrogen projectile plausibly moves with a bound electrons in LiF solid insulator target (28). Under such an assumption we could estimate the screening potential  $U_e^{(AD)} = 389.9 - 198.2 \sim 192$  eV. In the case of molecular  $\text{D}_2$  or  $\text{H}_2$  gas targets, as well, we could count the electron capture by projectile lithium ion.

The bare S-factors for the same reaction have been extracted using an indirect method, the Trojan-Horse Method through  ${}^6\text{Li}({}^6\text{Li}, \alpha\alpha){}^4\text{He}$  reaction (11). The comparison between direct and the indirect methods gives the screening potential  $U_e = 320 \pm 50$  eV. The corresponding enhancement factors are shown with the dash-dotted curve. The contrast between the direct measurement data and the theoretical estimation for the bare S-factor using  $R$ -matrix theory gives  $U_e = 240$  eV. It is shown with dotted line. The extracted  $U_e$  with the two different methods are larger than the adiabatic limit.

We simulate  ${}^6\text{Li}+d$  and  ${}^6\text{Li}+D$  cases only. In the figure 9 the open and closed squares show the enhancement factor for  ${}^6\text{Li}+d$  and  ${}^6\text{Li}+D$  reactions, respectively.

Again the average enhancement factors of the  ${}^6\text{Li}+D$  reaction are larger than those of the  ${}^6\text{Li}+d$ . The fit of the obtained average enhancement factors suggests the screening potentials  $U_e = 152.0 \pm 9.9$  eV for  ${}^6\text{Li}+d$  and  $U_e = 211.3 \pm 16.0$  for  ${}^6\text{Li}+D$ . The screening potential for the  ${}^6\text{Li}+d$  reaction in our simulation does not exceed the adiabatic limit nor extracted values using  $R$ -matrix theory and THM, but one for the  ${}^6\text{Li}+D$  verges on the extracted values using  $R$ -matrix theory.

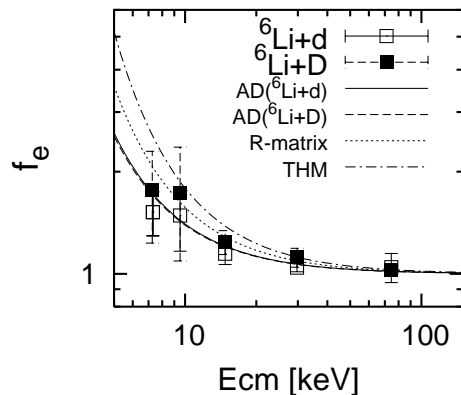


Fig. 9. same as Fig. 8 but for the  ${}^6\text{Li}+d$  and  ${}^6\text{Li}+D$  reactions.

Table 1

Comparison between the screening potential( $U_e$ ) in the adiabatic limit and in our CoMD simulation

|                 | $U_e(\text{keV})$ |             |              |                 |
|-----------------|-------------------|-------------|--------------|-----------------|
|                 | present results   | ref. (9)    | THM          | adiabatic limit |
| D+d             | $15.9 \pm 2.0$    | 8.7, 7.3    |              | 22.0*           |
| D+D             | $21.6 \pm 0.3$    |             |              | 37.1*           |
| $\text{He}^3+d$ | $83.2 \pm 1.2$    | 34, 60, 200 | $180 \pm 40$ | 119             |
| $\text{He}^3+D$ | $87.4 \pm 5.3$    |             |              | 110             |
| $\text{Li}^6+d$ | $152.0 \pm 9.9$   | 259, 248    | $320 \pm 50$ | 186             |
| $\text{Li}^6+D$ | $211.3 \pm 16.0$  |             |              |                 |

\* ref. (22)

In Table 1 we summarize our results of the screening potentials for each reaction and compare them with the extracted value using  $R$ -matrix theory and THM.

## 4 Summary

We discussed the effect of the screening by the electrons in nuclear reactions at the astrophysical energies. We performed molecular dynamics simulations with constraints and imaginary time for D+d, D+D,  ${}^3\text{He}+d$ ,  ${}^3\text{He}+D$ ,  ${}^6\text{Li}+d$ ,  ${}^6\text{Li}+D$  reactions. For all the reactions it is shown that both the average enhancement factors and their variances increase as the incident energy becomes lower. Using bare projectiles we obtained the average screening potential smaller than

the value in the adiabatic limit for all reactions. It is because of the excitation or emission of several bound electrons during the reactions. The comparison between bare and atomic projectile cases for each reactions revealed that the electron capture of the projectile guides to larger enhancements. The screening energies which are obtained by fits of average enhancement factors in the whole incident energy region for atomic projectile cases are in agreement with that extracted using  $R$ -matrix theory.

We performed numerical experiments using polarized targets for the  $D+d$  reactions. Using  $P_{\perp}$  targets we obtained relatively large enhancement with small variances, instead  $P_{\parallel}$  target gives large variance of the enhancement factor and relatively small averaged enhancement factor. It is because with the  $P_{\parallel}$  targets the force exerted from the electron to the relative motion of the nuclei is oscillational, in the direction of the beam axis, and the motion of the electron becomes often excited or unstable. It is the case where the chaoticity of the electron motion affects the tunneling probability and at the same time the enhancement factor of the cross section.

## Acknowledgments

We acknowledge valuable discussions and suggestions with Profs. T. Motoyoshi, T. Maruyama, A. Ono, C. Spitaleri and N. Takigawa.

## References

- [1] W.A.Lin and L.E. Ballentine, *Phys. Rev. Lett.* **65** (1990) 2927; O. Bohigas, S. Tomosvic, and D. Ullumo, *Phys. Rev. Lett.* **65** (1990)5; A. Shudo, and K.S.Ikeda, *Phys. Rev. Lett.* **74** (1995) 682.
- [2] S. Kimura, and A. Bonasera, *Phys. Rev. Lett.* **93** (2004) 262502.
- [3] A. Krauss, H. W. Becker. H. P. Trautvetter, and C. Rolfs, *Nucl. Phys. A* **467** (1987) 273;
- [4] S. Engstler *et al.*, *Phys. Lett. B* **202** (1988) 179.
- [5] L. Bracci, G. Fiorentini, V.S. Melezhik, G. Mezzorani, and P. Quarati, *Nucl. Phys. A* **513** (1990) 316.
- [6] C. Rolfs, and E. Somorjai, *Nucl. Instrum. Meth. B* **99** (1995) 297.
- [7] H. Yuki *et al.*, *JETP Lett.* **68** (1998) 823.; F. Raiola, *et al.*, *Phys. Lett. B* **547** (2002) 193.
- [8] M. Junker, *et al.*, *Phys. Rev. C* **57** (1998) 2700.
- [9] F. C. Barker, *Nucl. Phys. A* **707** (2002) 277.
- [10] M. Lattuada, *et al.*, *Astrophys. J.* **562** (2001) 1076 .
- [11] A. Musumarra, *et al.*, *Phys. Rev. C* **64** (2001) 068801.
- [12] T. D. Shoppa, S. E. Koonin, K. Langanke, and R. Seki, *Phys. Rev. C* **48** (1993) 837.

- [13] S. Kimura, N. Takigawa, M. Abe, and D.M. Brink, *Phys. Rev. C* **67** (2003) 022801(R).
- [14] T. D. Shoppa, *et al.*, *Nucl. Phys. A* **605** (1996) 387.
- [15] M. Papa, T. Maruyama, and A. Bonasera, *Phys. Rev. C* **64** (2001) 024612.
- [16] S. Kimura, and A. Bonasera, physics/0409008.
- [17] H. J. Assenbaum and K. Langanke and C. Rolfs, *Z. Phys. A* **327** (1987) 461.
- [18] D. D. Clayton, *Principles of Stellar Evolution and Nucleosynthesis* (University of Chicago Press, 1983) Chap. 4.
- [19] J. Makino, and S. J. Aarseth, *PASJ* **44** (1992) 141.
- [20] A. Bonasera, and V. N. Kondratyev, *Phys. Lett. B* **339** (1994) 207; T. Maruyama, A. Bonasera, and S. Chiba, *Phys. Rev. C* **63** (2001) 057601.
- [21] J.W. Negele, *Nucl. Phys. A* **502** (1989) 371.
- [22] Y. Kato, N. Takigawa, nucl-th/0404075.
- [23] F. Sattin, and L. Salasnich, *Phys. Rev. E* **59** (1999) 1246; F. Sattin, and L. Salasnich, *J. Phys. B*, **29** (1996) L699.
- [24] K. Langanke, T.D.Shoppa, C.A.Barnes, and C.Rolfs, *Phys. Lett. B* **369** 211(1996).
- [25] M. Aliotta, *et al.*, *Nucl.Phys.A* **690**, 790(2001).
- [26] M. La Cognata, *et al.*, to be published in *Nucl. Phys. A*
- [27] T. Geyer and J. M. Rost, *J. Phys. B: At. Mol. Opt. Phys.* **36** L107(2003). and references there in.
- [28] K. Eder, *et al.*, *Phys. Rev. Lett.* **79** 4112(1997); P. Roncin, *et al.*, *Phys. Rev. Lett.* **83** 864(1999)